MOLECULAR GAS AND THE HOST-GALAXY SYSTEM OF THE $z \sim 0.3$ QSO PG 1700+518

A. S. EVANS[1,9,10,11,12], D. C. HINES[2], P. BARTHEL[3], G. SCHNEIDER[4], J. A. SURACE[5], D. B. SANDERS[6], T. VAVILKIN[1,9],
D. T. FRAYER[7], L. J. TACCONI[8], AND L. J. STORRIE-LOMBARDI[5]

[1] Department of Physics and Astronomy, Stony Brook University, Stony Brook, NY 11794-3800, USA; tvavilk@vulcan.ess.sunysb.edu
[2] Space Science Institute, 4750 Walnut St., Suite 205, Boulder, CO 80301, USA; dhines@as.arizona.edu
[3] Kapteyn Astronomical Institute, P.O. Box 800, Groningen, AV9 700, The Netherlands; pdb@astro.rug.nl
[4] Steward Observatory, The University of Arizona, 933 North Cherry Avenue, Tucson, AZ 85721, USA; gschneider@as.arizona.edu
[5] Spitzer Science Center, Pasadena, CA 91125, USA; jason@ipac.caltech.edu, lisa@ipac.caltech.edu
[6] Institute of Astronomy, University of Hawaii, 2680 Woodlawn Dr., Honolulu, HI 96822, USA; sanders@ifa.hawaii.edu
[7] Infrared Processing and Analysis Center, California Institute of Technology, MS 100-22, Pasadena, CA 91125, USA; frayer@ipac.caltech.edu
[8] Max-Planck Institut fur extraterrestrische Physik, Giessenbachstrasse, Garching D-85748, Germany; linda@mpe.mpg.de
Received 2008 April 11; accepted 2009 April 25; published 2009 June 10

ABSTRACT

The detection of CO(1→0) emission in the massive (i.e., $M_H \sim -26.13$ mag), $z \sim 0.3$ host-galaxy system of the broad absorption line quasi-stellar object (QSO) PG1700+518 is reported. The host system has a CO luminosity of $L'_{CO} \sim 1.4 \times 10^{10}$ K km s^{-1} pc^2, and thus a star-forming molecular gas mass of $M(H_2) \sim 6 \times 10^{10}$ $M_\odot$ (adopting an $\alpha = 4$ $M_\odot$ [K km s^{-1} pc^2]$^{-1}$), making it one of the most molecular gas-rich Palomar-Green QSO hosts observed to date. New *Hubble Space Telescope* WFPC2 direct and NICMOS coronagraphic images show the highest resolution view yet of the host and companion. The new NICMOS image reveals the underlying, apparently tidally disrupted structure seen previously from high-resolution ground-based optical imaging. Light from the host galaxy is overwhelmed by the central point source in the WFPC2 images. The companion galaxy is well resolved in both data sets, and the WFPC2 provides for the first time a clear picture of the optically visible ring structure. The CO redshift is within the range of redshifts derived from optical QSO emission lines, thus the observed CO is associated with the QSO host. However, it cannot be ruled out that the companion has at least $\sim 10^{10}$ $M_\odot$ of molecular gas. Finally, if the far-infrared luminosity, which is 1/5 of the bolometric luminosity, is the luminosity of the starburst population, the star formation rate is estimated to be ~ 210 $M_\odot$ yr^{-1}. There is thus sufficient molecular gas in the QSO host galaxy to fuel both star formation and QSO activity for another $\sim 10^8$ yr. We speculate that we may be witnessing the fueling event in progress that resulted from a collision between the QSO host and the companion galaxy, and that there is an accompanying expulsion of material along our line of sight in the form of broad absorption line gas.

Key words: galaxies: active – galaxies: individual (PG1700+518) – galaxies: interactions – galaxies: ISM –
infrared: galaxies – ISM: molecules – quasars: emission lines

Online-only material: color figures, FITS file

1. INTRODUCTION

The inherent brightness of quasi-stellar objects (QSOs) has made observations of their host galaxies a challenge. Ever improving observing techniques and the availability of adaptive optics and space-based instrumentation have enabled more effective modeling of image point-spread functions (PSFs) and more accurate subtractions of the QSO nucleus from the underlying host. The result of these efforts is that QSO host galaxies are now known to be diverse in morphology (e.g., Bahcall et al. 1995; McLeod & McLeod 2001; Surace et al. 2001; Veilleux et al. 2006), in contrast to the original belief that luminous QSOs resided only in giant elliptical galaxies (e.g., Kristian 1973; Silk et al. 1973; Hawkins 1978). In addition, observations of the rotational transitions of CO, accessible with millimeter-wave telescopes, have proven to be an effective

tool for studying QSO hosts. Millimeter-wave CO surveys of Palomar-Green QSOs (PG QSOs; Schmidt & Green 1983) over the last few decades have provided evidence that many QSO host galaxies are rich in star-forming molecular gas (e.g., Evans et al. 2001, 2006; Scoville et al. 2003). The combination of optical/ near-infrared (NIR) and millimeter wavelengths provide the best opportunity for a well rounded picture of the nature of QSO host galaxies and the activity occurring in them, and in the past have proven to be an effective tool for differentiating between gas-poor elliptical hosts and gas-rich advanced mergers (Evans et al. 2001; Scoville et al. 2003).

The QSO PG 1700+518 is a member of a rare class of low-ionization, broad absorption line QSOs and is the most luminous radio-quiet member of the optically selected PG QSO sample in the local universe (i.e., $z \lesssim 0.3$). The host system has an infrared luminosity of $L_{IR}(8-1000 \ \mu m) \sim 4.8 \times 10^{12}$ $L_\odot$ (see Section 4) and a bolometric luminosity of $L_{bol} \sim 6.2 \times 10^{12}$ $L_\odot$.[13] It has been the subject of several imaging investigations, in part, due to a large companion galaxy located 1″.6 (7 kpc) north of the QSO host (e.g., Stockton et al. 1998; Hines et al. 1999; Guyon et al. 2006). Based on their *Hubble Space Telescope* (*HST*)/

---

[13] Estimated from the L_{IR} and the value of $L_{IR}/L_{0.1-1\mu m} = 0.76$ in Guyon et al. (2006). Note that this estimation does not factor in emission blueward of 0.1 μm.

NICMOS 1.6 μm imaging of the PG 1700+518 system, Hines et al. ([1999](#)) proposed that the companion galaxy is a $2L^*$ ring galaxy produced by a near head-on collision with the QSO host, and that the putative low impact parameter was responsible for energizing the QSO nucleus and producing the extreme infrared emission. Canalizo & Stockton ([1997](#)) and Stockton et al. ([1998](#)) have made use of Keck spectroscopy to conclude that the companion contains an old stellar population plus a young 85 Myr component. They measure a redshift, z, = 0.2929 for the companion (compared with z range of ~ 0.286–0.292 for the QSO: see Section [2.1](#)), clearly associating the companion with the QSO host.

In this paper, CO(1→0) observations of the PG 1700+518 system are presented. The presently reported detection of molecular gas has been obtained as part of a volume-limited ($z \lesssim 0.3$) CO(1→0) survey of PG QSO hosts (A. S. Evans et al. 2009, in preparation). In addition, new *HST*/*WPFC2* direct and *NICMOS* coronagraphic images are presented; these data show the clearest view to date of the QSO host galaxy and its companion (collisional) ring galaxy. It is argued that the observed CO emission is associated with the QSO host. A $H_0 = 75$ km s^{-1} Mpc^{-1}, $\Omega_m = 0.3$, and $\Omega_\Lambda = 0.7$ cosmology is adopted; at the redshift of PG 1700+518, 4.06 kpc subtends $1''$ on the sky.

2. OBSERVATIONS AND DATA REDUCTION

2.1. Millimeter Data

Observations of the redshifted CO(1 → 0) emission in the host-galaxy system of PG 1700+518 were done at the IRAM 30 m telescope during the 2006 April–May observing period. Both 3 mm receivers were tuned to the frequency 89.2192 GHz, which is the frequency the CO(1 → 0) emission was expected to correspond to based on the optical redshift of $z_{\rm optical} = 0.2920$ in Schmidt & Green ([1983](#)). The receivers were used in combination with the filterbanks, providing a total bandwidth of 512 MHz for the observations. During the observations, the pointing was monitored by observing standard continuum sources.

Scans were intermittently averaged together during the observations with the IRAM data reduction package CLASS to check for line emission. The QSO host was observed during two separate transits, with a total on-source integration time of 49 minutes and 87 minutes. During the first set of observations, an apparent emission line was observed with an amplitude peak at 500 km s^{-1} blueward of the velocity corresponding to the optical redshift (i.e., $z_{\rm optical} = 0.2920$). For the second set of observations, the receivers were tuned to 89.3700 GHz ($z = 0.290$). With the second tuning, a 6σ CO emission line was observed to be centered in the bandpass. The redshift of the CO(1→0) emission line is within the range of optical emission-line redshifts (= 2.86–2.92) derived for the QSO based on Fe II, [O III], and Mg II and hydrogen recombination lines; the average optical redshifts measured by Pettini & Boksenberg ([1985](#)) and Stirpe ([1990](#)) are 0.288 and 0.290, respectively. The redshift is also consistent with that of a 2.5σ detection of the CO(3→2) emission line previously and independently obtained with the James Clerk Maxwell Telescope at an observed frequency of 268.05 GHz (P. Barthel 2007, unpublished; see also Papadopoulos et al. [2008](#)).

After the scans from the second tuning were averaged together, a linear baseline was subtracted outside the velocity range of the CO line emission. The amplitudes of the spectrum were converted to main beam brightness temperature, $T_{\rm mb}$, by
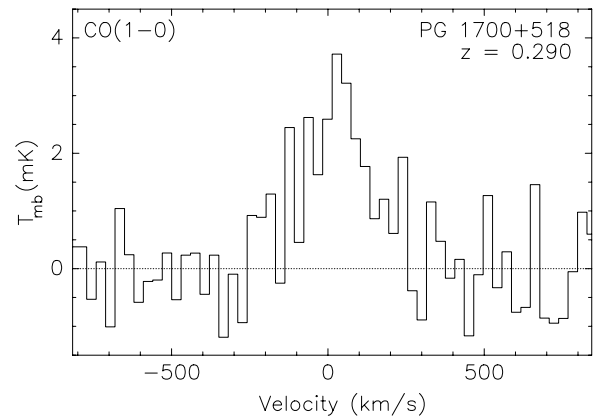

Figure 1. IRAM 30 m Telescope spectra of CO(1 → 0) emission from the host-galaxy system PG 1700+518. The intensity scale is in units of main beam brightness temperature. A linear baseline has been subtracted from the spectrum; the baseline subtraction is performed outside of the velocity range of the emission line. The redshift corresponding to the zero velocities of the spectrum is $z = 0.290$.

multiplying the spectrum by the ratio of the forward-to-beam efficiencies of the telescope at 89 GHz (= 1.218), then the spectrum was smoothed to ~ 20 km s^{-1}. The resultant spectrum is shown in Figure [1](#). Finally, the CO line flux was measured by numerically integrating over the channels in the line profile, and the line width was measured as FWHM.

2.2. NICMOS Coronagraphic Imaging

HST/NICMOS coronagraphic observations of PG1700+518 in the F160W filter (similar to H band with $\lambda_{\rm cent} = 1.594$ Å, FWHM = 0.403 Å.) were obtained as part of the *HST* Cycle 7 GTO program 7220 (PI: R. Weynman), which was designed to reveal the host galaxies of QSOs. The QSO PG1718+481 ($z = 1.084$) was also observed as part of the same program, and has been processed in the same manner as PG1700+518 to provide as a validity check on our image processing.

Even with the coronagraphic rejection of significant underlying instrumentally diffracted and scattered light from the central, unresolved QSO nucleus, it is necessary to subtract a well matched template point-spread function (PSF) to further enhance the image contrast and reveal structure close to the nucleus. In the case of PG1718+481, a stellar PSF star (2MASS J17193256+4804193, hereafter 2MJ1719) with similar $J - H$ color index was observed contemporaneously, but no PSF template was specifically programmed for PG1700+518. Serendipitously, observations of a template PSF star (HD 102970) for another QSO target were executed only one day following the observations of PG1700+518. This short time span suggested that HD 102970 might be a good PSF template for PG1700+518, because potentially problematic secular changes in the fine structure of the NICMOS coronagraphic PSF structure had been noted on timescales of months throughout HST Cycle 7 (e.g., see Schneider et al. [1999](#)). The observations of the PSF template stars and the QSOs are summarized in Table [1](#).

The raw imagery of the QSOs and the PSF template stars have been recalibrated following the prescription in Schneider et al. ([2005](#)), but with calibration data appropriate for *HST* Cycle 7 and employing methods adopted in the *Hubble* Legacy Archive program AR 11279 (PI: G. Schneider). The instrumentally calibrated count-rate images of each object have been reconstructed from the raw MULTIACCUM frames, and median combined them into a final image (as shown in panels

Table 1
NICMOS & WFPC2 Observation Summary

Visit[a]	Target	H mag[b]	Date Obs	Orient[c]	Type[d]	Readout Mode[d]	ExpTime[e]	Exp[f]	Datasets[g]
04	PG1700+518	13.02[h]	1998 Jul 20	285.51	NIC2/ACQ	ACQ (ACCUM)	60 s	2	n4fh04djq
					NIC2/CORON	STEP64/NSAMP18	639.94 s	4	n4fh04010*
				195.91	PC1/IMAGE	CR-SPLIT=NO	1000 s	2	u4fha402r+
05	PG1718+4807	13.05	1998 Jul 21	275.66	ACQ	ACQ (ACCUM)	60 s	2	n4fh05k3q
					CORON	STEP64/NSAMP18	639.94 s	4	n4fh05010*
					CORON	STEP64/NSAMP19	703.94 s	4	n4fh05020*
					CORON	STEP64/NSAMP22	895.93 s	1	n4fh05knq
05	J171938.3+480412 16	11.24	1998 Jul 21	276.65	ACQ	ACQ (ACCUM)	15 s	2	n4h05ktq
					CORON	STEP2/NSAMP20	33.89 s	4	n4fh05040*
08	HD 102970	7.56	1998 Sep 26	127.81	ACQ	ACQ (ACCUM)	0.64 s	2	n4fha8ztq
					CORON	SCAMRR/NSAMP22	4.466 s	4	n4fha8010*

Notes.
[a] *HST* /GO 7220 Visit ID number.
[b] 2MASS H magnitudes from Skrutskie et al. (2006).
[c] Position angle (degrees) of image +Y-axis (east of north).
[d] See Barker et al. (2007) and Heyer et al. (2004) for NICMOS and WFPC2 image/readout modes and filters.
[e] Exposure time for each exposure (before combining).
[f] Number of exposures.
[g] *HST* archive data set ID; * indicates that the data set ID is an association, but observer should extract the images separately; + the first image in nonassociated data set.
[h] $V = 15.2$; Hutchings et al. (1984)

(A) − (E) of Figure 2) after verifying the inter-image stability and repeatability of the individual contributing frames.

Figure 2 shows the subsequent PSF subtraction procedure. The intensity of the 2MJ1719 PSF image was renormalized (separately) to match the Two Micron All Sky Survey (2MASS) *H*-band magnitudes of each QSO and subtracted after astrometric registration (accurate to ∼5 mas; Schneider et al. 1999) from the occulted targets (Figure 2: (A) minus (C), and (B) minus (C)). Unfortunately, the PSF-subtracted images each have a negative "hole" caused by a previously unknown, much fainter ($H = 17.63$, $\Delta H = +6.39$) point source 1″6 to the south (to the "right" of the coronagraphic obscuration in Figure 2(C)) of 2MJ1719. Even with this negative imprint, no flux density excesses or deficits (indicative of an ill-matched PSF template) are seen in the PG1718+481 minus 2MJ1719 image ((B) − (C)) within 3″3 of the occulted QSO (i.e., the host galaxy of PG1718+481 was not detected). The sensitivity of this ((B) − (C)) difference image may be gauged in noting three faint and moderately extended (extragalactic) sources ≈3″9 to the east of PG1718+481 ("below" the coronagraphic obscuration). The central, and brightest, of these sources has an *H*-band magnitude of ≈ 20.2. The PG1700+518 minus 2MJ1719 image ((A) − (C)) reveals the host galaxy of the occulted QSO and the ringlike companion galaxy (Hines et al. 1999), but the negative hole cuts out some of the light from the host galaxy.

The efficacy (in the non-photon-noise-dominated regions) of the (B) − (C) and (A) − (C) PSF subtractions is also limited by the (low) signal-to-noise ratio (S/N) of the 2MJ1719 image. To alleviate both issues, we evaluated the use of HD 102970 as PSF template (Figure 2: (A) − (D), (B) − (D)). Though both the PG1700+518 host galaxy and the ringlike companion galaxy are revealed, a negative imprint due to a mismatch in PSF structure appears to the west of the QSO ("above" the coronagraphic obscuration) along with lower intensity radially directed residuals at several other circum-hole azimuths. These artifacts have the signatures of PSF subtraction residuals induced by the motions of both the NICMOS camera 2 cold pupil mask and "breathing" of the *HST* optical telescope assembly (see Krist et al.

1998; Schneider et al. 1999). This (A) − (D) subtraction further confirms the existence of the structures seen in PG1700+518 ((A) − (C)), but is of lesser quality due to the systematic differences in the underlying PSF structures.

Noting that the PG1718+481 minus 2MJ1719 image ((B) − (C)) is very clean of PSF-subtraction residuals, and does not show evidence for extended structure from the PG1718+481 host galaxy, an attempt was made to use PG1718+481 as a PSF for PG1700+518. This results in a PSF subtraction that is essentially identical to the PG1700+518 minus 2MJ1719 ((A) − (C)) image, but with higher S/N and no negative "holes" near the object. Hence, the analysis to follow is done using the PG1700+518 minus PG1718+481 image exclusively. The final coronagraphic image is shown in Figure 3. Although the coronagraphic hole has a 0″3 radius, residual artifacts from the PSF-subtraction dominate within 0″4.

2.3. WFPC2 Imaging

Optical (F547M) images of PG1700+518 were also obtained with WFPC2 as part of the *HST* Cycle 7 GTO program 7220 (PI: R. Weymann). Two separate 1000 s images with a small angle offset were obtained to mitigate bad pixels and eliminate cosmic rays. The data were initially processed through the STScI on-the-fly pipeline to obtain calibrated images. Both images were then cleaned, first with the *jcrrej2* routine (Rhoads 2000) and then with the *lacosim* routine (van Dokkum 2001). These cleaned images were combined using the *imcombine* task in IRAF,[14] taking into account astrometric offsets determined by centering on the QSO. Any remaining cosmic rays were identified by eye and replaced using *imedit*. The final image suffers from saturation in the central pixels, but clearly reveals the ringlike companion galaxy.

Despite the saturation, PSF subtraction was attempted using a TinyTIM PSF model scaled to remove the diffraction spikes.

---

[14] IRAF is distributed by the National Optical Astronomy Observatories, which are operated by the Association of Universities for Research in Astronomy, Inc., under cooperative agreement with the National Science Foundation.
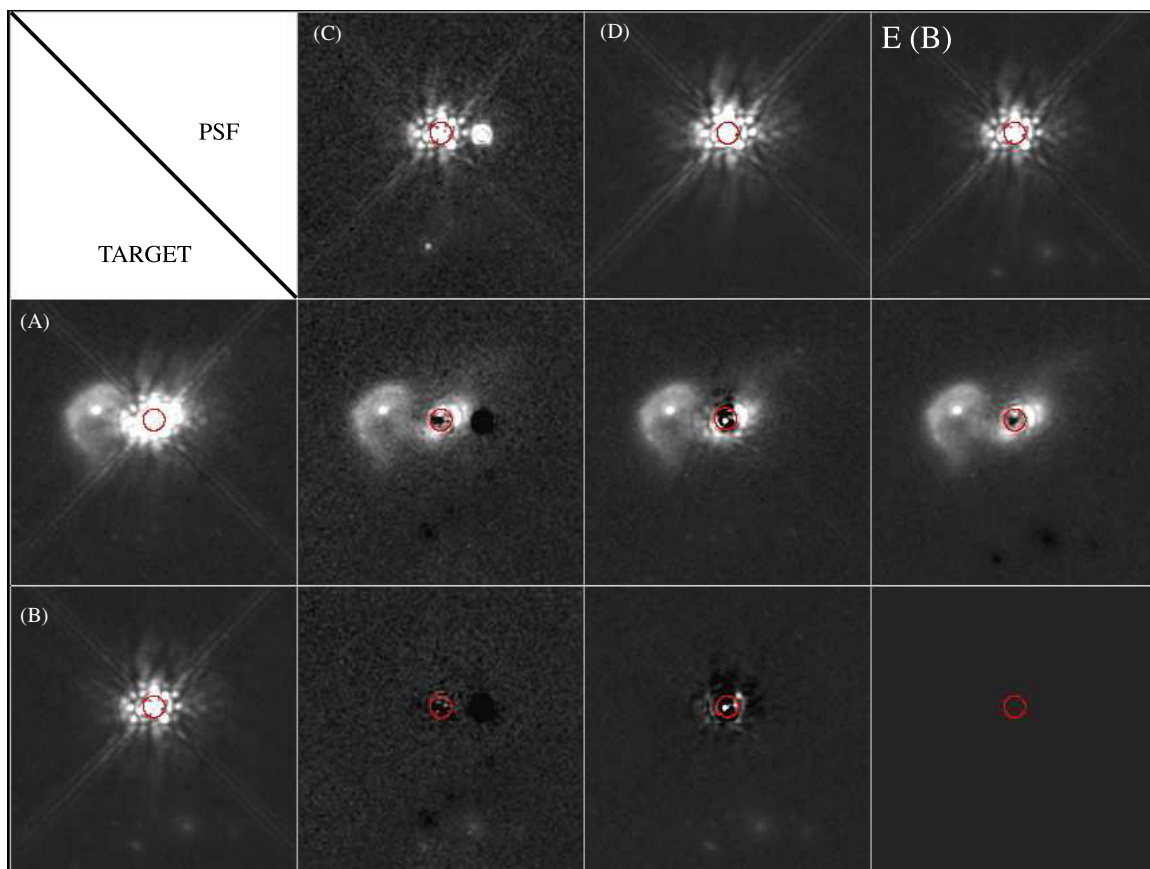
Figure 2. NICMOS coronagraphic images of the QSOs PG1700+518 and PG1719+481 ((A) & (B)) and the point-source PSF templates 2MASS J17193256+4804193 and HD 102970 ((C) & (D)). Panel (E) is also the QSO PG1719+481, which is indistinguishable from a point source, and is therefore used for PSF subtraction of PG1700+518 (see Section 2.2). PSF subtractions using the PSFs in the top row are shown for each QSO (e.g., (A) − (C), (A) − (D), (A) − (E)). All images are $8'' \times 8''$(105×105 pixel) extracts from the $19''.2 \times 19''.3$ (256×256 pixel) NICMOS camera 2 field and have been scaled (renormalized) in intensity to the H-band flux density of PG 1700+518 ($H = 13.02$). The red circles represent the $0''.3$ radius coronagraphic obscuration. All images are shown with a linear display stretch from -0.05 to $+0.4$ renormalized counts s^{-1} pixel^{-1}. Note that the images are presented in NICMOS detector coordinates, which fixes the PSF structure on the page allowing for easy comparison between objects and observations.

(A color version of this figure is available in the online journal.)
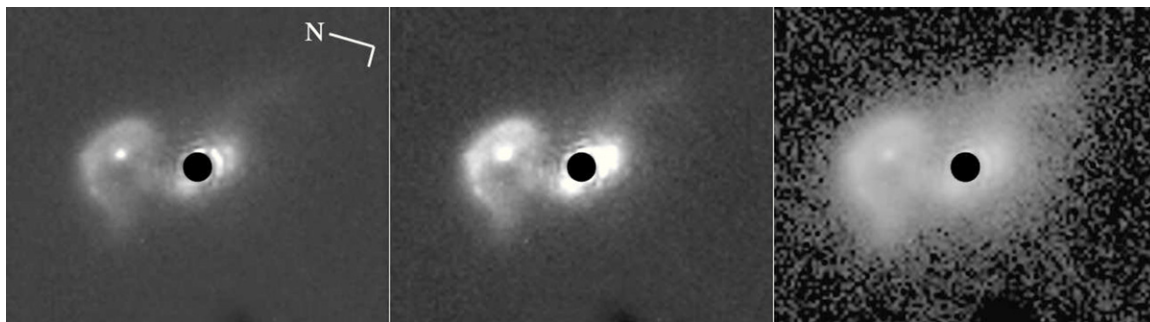

Figure 3. Morphology and extent of the PG1700+518 host (at $r > 0''.3$ from its nucleus) and companion ring galaxies are revealed in these three images shown with different dynamic display ranges. Left: linear display stretch from -0.1 to $+0.5$ counts s^{-1} pixel^{-1}. Middle: linear display stretch from -0.05 to $+0.3$ counts s^{-1} pixel^{-1}. Right: $\log_{10}$ display stretch from $[-0.3]$ ro $[+0.2]$ counts s^{-1} pixel^{-1}.

(A FITS version of this figure is available in the online journal.)

The TinyTIM model was four times oversampled, and was generated with a spectral slope $F_\nu \propto a^{-0.6}$. This is near the median spectral slope for PG QSOs given by Neugebauer et al. (1987; see also Surace et al. 2001) for the optical continuum. Several other spectral slopes were also tested, but none were more effective. The residuals seen in the PSF-subtracted image are a combination of Poisson noise, oversubtraction of the saturated core, and PSF model mismatches likely due to the "breathing" modes of *HST*. Both the total intensity image and the PSF-subtracted image are shown in Figure 4.

3. RESULTS

3.1. Millimeter Data

The CO(1→0) emission-line spectra of the PG 1700+518 system (Figure 1) has a $\Delta v_{\mathrm{FWHM}} \sim 260$ km s^{-1}, and the CO line
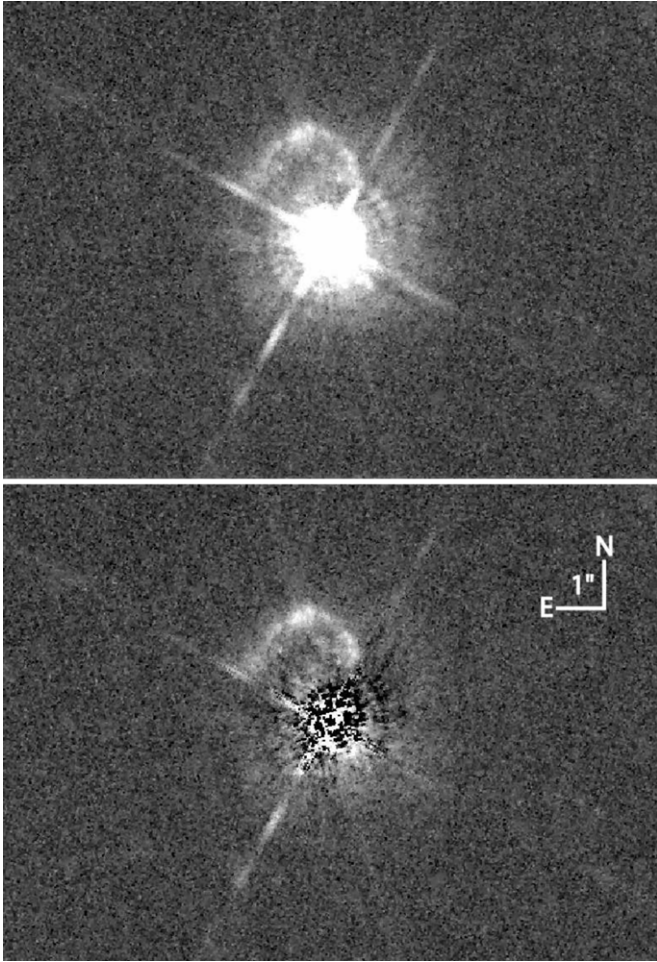
Figure 4. Two views of the *HST*/WFPC2 image of the PG 1700+518 system. The image on bottom has been PSF-subtracted using a spectrally matched TinyTIM PSF. In this rendering, north is up, east is to the left, and the images are shown with a linear stretch.

intensity is $T_{mb}\Delta v \sim 0.79 \pm 0.14$ K km s^{-1}. The CO luminosity of $L'_{CO} = 1.4(\pm 0.2) \times 10^{10}$ K km s^{-1} pc^2 is calculated via

$$L'_{CO} = 2.4 \times 10^3 \left(\frac{S_{CO}\Delta v}{\text{Jy km s}^{-1}} \right) \left(\frac{D_L}{\text{Mpc}} \right)^2 \frac{1}{(1+z)} \text{K km s}^{-1} \text{ pc}^2,$$

(1)

where $S_{CO}\Delta v$ ($= 3.9 \pm 0.7$ Jy km s^{-1}) is the CO(1→0) flux obtained by multiplying the line intensity by the conversion factor for an unresolved source (i.e., $S/T_{mb} = 4.95$ J K^{-1}), and D_L ($= 1394$ Mpc) is the luminosity distance. The molecular gas mass, $M(H_2)$, is calculated by adopting the conversion factor $\alpha = M(H_2)/L'_{CO} \sim 4$ $M_\odot$ (K km s^{-1} pc^2)$^{-1}$ (see Evans et al. 2001 for a detailed discussion of α), and is estimated to be $5.7(\pm 1.0) \times 10^{10}$ $M_\odot$.

3.2. HST Data

Figure 5(a) and 5(b) shows the PSF-subtracted WFPC2 and NICMOS images side by side. The WFPC2 direct and NICMOS coronagraphic images of the PG 1700+518 system show the general features revealed in previously published data (Hutchings et al. 1992; Stickel et al. 1995; Stockton et al. 1998; Hines et al. 1999; Márquez et al. 2001; Guyon et al. 2006). In particular, both the WPFC2 and NICMOS images reveal the nucleus and bright NW arc associated with the outer "ring" of the companion galaxy. The NICMOS image also shows the

extended, presumably tidal structure extending from the QSO host galaxy to the SW seen previously in optical (Stickel et al. 1995; Stockton et al. 1998) and NIR (Guyon et al. 2006) images including the direct PSF-subtracted 1.6 μm NICMOS images presented by Hines et al. (1999); this extension from the host galaxy is not detected in the WFPC2 image. In addition, the new images provide better separation of QSO host-galaxy emission from that of the companion, and provide new information on the color of the ring structure in the companion galaxy. The images are discussed in more detail below.

The NICMOS PSF-subtracted, coronagraphic image shows the PG 1700+518 system to be comprised of two galaxies separated by 6.7 kpc ($= 1\farcs6$). Beyond the $0\farcs4$ ($= 1.2$ kpc) radius, the galaxy hosting the QSO consists of a high surface brightness elongated "bulge," the SW portion of which corresponds with the "knot" of emission seen in the adaptive optics images (e.g., Márquez et al. 2001; Guyon et al. 2006). There is a hint of this feature in the WFPC image, but the region is corrupted by residuals in the PSF subtraction. There is also fainter emission in the NICMOS image extending to the SW, which appears to be the aforementioned "tidal" tail. The new NICMOS image shows this structure more clearly than in previous data, and traces the emission to 12.2 kpc ($= 3\farcs0$). The total integrated magnitude of the host-galaxy emission in the NICMOS image is $m_H = 15.9$, 1.3 magnitudes smaller than that derived by Guyon et al. (2006), due to the loss of flux in the NICMOS coronagraphic hole.[15]

There is no obvious correlation between any of the structures revealed in the NICMOS image with those in the 6 cm and 20 cm radio images (Hutchings et al. 1992). Except for possible emission at the location of the SW emission "knot" seen in the NIR, none of the other structures associated with the QSO host galaxy are detected in the WFPC2 image. Neither the WFPC2 nor the NICMOS images shows evidence for the putative "jet" hinted at in the optical images of Hutchings et al. (1992).

The NICMOS image of the companion galaxy shows a $\sim$15 kpc long semicircular ridge of emission surrounding an off-centered "blob" of emission, which is presumably the nucleus of the companion if it is indeed a collisional ring galaxy. The putative companion nucleus is relatively bright in the NICMOS F160W image, but barely visible in the WFPC2 image. Using a $0\farcs23$ radius circular aperture centered on the location of the peak emission as measured in the NICMOS image, and applying a point-source aperture correction as outlined in Holtzman et al. (1995), the F547M magnitude of the companion nucleus is $m_{F547M} = 23.7$ mag (Vega). Given its NICMOS F160W magnitude of $m_{F160W} = 19.1$ mag (Vega), the $m_{F547M} - m_{F160W} \sim 4.6$ mag, indicating that the companion nucleus is very red.

The "ring" component of the companion is bluer, with integrated magnitudes $m_{F547M} \approx 20.1$ mag and $m_{F160W} \approx 17.6$ mag, and $m_{F547M} - m_{F160W} \sim 2.8$ mag. In the rest frame these colors are similar to the $B - J$ colors of normal galaxies (e.g., Griersmith et al. 1982; Persson et al. 1979). These colors are also similar to the integrated colors of collisional ring galaxies ($\langle B - J \rangle \sim 2.2 \pm 0.7$; Hines et al. 1999; Appleton & Marston 1997), but about a magnitude redder than their outer rings ($\langle B - J \rangle \sim 1.9 \pm 0.8$; Appleton & Marston 1997).

At both wavelengths, it is clear that the emission from the ring terminates sharply at the "outer" boundary (i.e., the edge farthest

---

[15] We forgo the traditional "radial profile fitting" exercise owing to the clearly asymmetric, and complicated morphology of the system. Instead, we provide the actual FITS file for use by interested parties for modeling (available in the online journal).
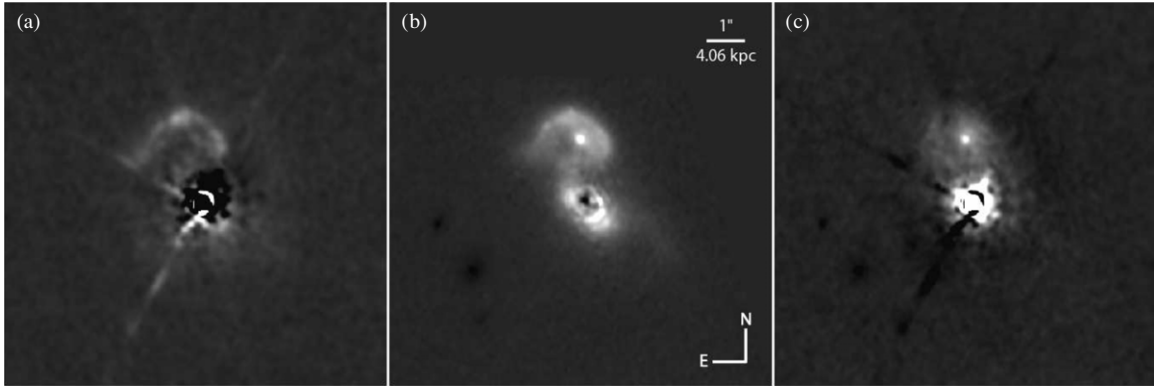
Figure 5. Comparison between the WFPC2 (a) and NICMOS (b) PSF-subtracted images of PG 1700+518. Panel (c) shows the difference image (b–a) produced by subtracting the WFPC2 image scaled to null the ring in the NICMOS image. In this rendering, north is up, east is to the left, and the images are shown with a linear stretch.

from the putative companion nucleus). Figure 5(c) also presents an image produced by subtracting the WFPC2 image (smoothed to the NICMOS resolution) from the NICMOS image, with the amplitude of the WFPC2 image scaled to null the ring. The resulting image retains the nucleus of the companion surrounded by smooth, radially decreasing surface brightness terminating near the semicircle ridge of the ring (the radial surface brightness profile is equally well fit by an exponential or $R^{1/4}$ law over this spatial scale). The sharpness of the outer boundary in both optical and NIR, and the smoothly decreasing residual NIR surface brightness, are both consistent with that seen in other collisional ring galaxies (e.g., Marston & Appleton 1995; Appleton & Marston 1997).

It is worth noting that there has recently been some speculation that the ring structure could be a shell structure produced by Super- and Hyper-Nova explosions (Lipari et al. 2009). However, as discussed in Hines et al. (1999), the morphology of the companion is strikingly similar to collisional ring galaxies in general and is nearly identical in appearance to the collisional ring galaxy WN1 (Appleton & Marston 1997). The new WFPC2 data, combined with the new NICMOS results, further support this interpretation.

4. ESTIMATION OF THE NEAR-INFRARED AND FAR-INFRARED LUMINOSITIES OF THE PG 1700+518 SYSTEM

In the discussion section to follow, the near- and far-infrared (FIR) luminosities, L_{IR} and L_{FIR}, respectively, are used to draw conclusions about the PG 1700+518 system. This section contains a brief description of the manner in which both quantities were calculated.

Sanders & Mirabel (1996) provide a table of standard definitions of infrared flux densities and luminosities. Based on their prescriptions, the infrared luminosity of the PG 1700+518 system, estimated over the wavelength range 8–1000 μm, is

$$L_{IR} = 1.7 \times 10^5 \pi \left(\frac{D_L}{Mpc}\right)^2 \times \left[13.48\left(\frac{f_{12\,\mu m}}{Jy}\right)\right.$$
$$\left. + 5.16\left(\frac{f_{25\,\mu m}}{Jy}\right) + 2.58\left(\frac{f_{60\,\mu m}}{Jy}\right) + \left(\frac{f_{100\,\mu m}}{Jy}\right)\right] L_\odot$$
$$= 4.8(\pm0.6) \times 10^{12} L_\odot, \qquad (2)$$

where $f_{X\,\mu m}$ is the flux density at the rest-frame wavelength X μm. The $f_{X\,\mu m}$ are derived from *Spitzer Space Telescope* and
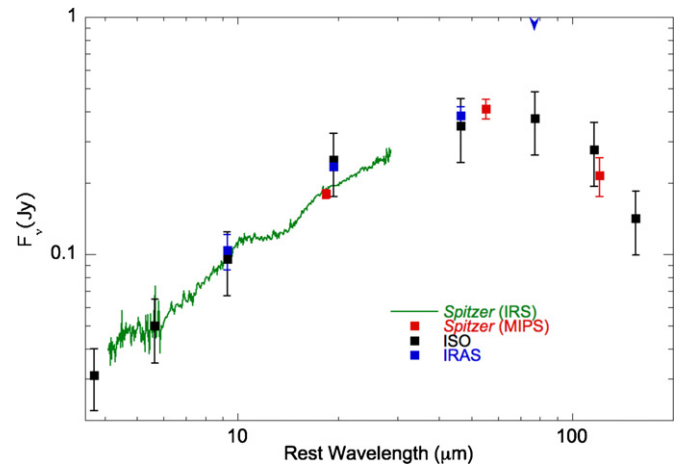

Figure 6. Spectral energy distribution of the PG 1700+518 system. Plotted data are from *IRAS*, *ISO*, and *Spitzer Space Telescope*. The IRS spectrum is from Shi et al. (2007), and the MIPS photometry is from D. Hines 2009, private communication.

(A color version of this figure is available in the online journal.)

Infrared Space Observatory (ISO) data. The FIR luminosity, estimated over the wavelength range 40–120 μm, is

$$L_{FIR} = 1.2 \times 10^5 \pi \left(\frac{D_L}{Mpc}\right)^2 \left[2.58\left(\frac{f_{60\,\mu m}}{Jy}\right) + \left(\frac{f_{100\,\mu m}}{Jy}\right)\right] L_\odot$$
$$= 1.0(\pm0.1) \times 10^{12} L_\odot. \qquad (3)$$

Note that the L_{FIR} is sometimes calculated over the luminosity range 40–500 μm, which requires an additional scale factor (= 1.4–1.8) that accounts for the emission redward of 120 μm.

As a double check of these values, all of the available mid-infrared (MIR) and FIR photometric data of the PG 1700+518 system were compiled—the resultant spectral energy distribution is shown in Figure 6. The $L_{8-155\,\mu m}$ and $L_{40-120\,\mu m}$ were measured by integrating under the spectral energy distribution (SED) from 8–155 μm and 40–120 μm, and yielded luminosities of $4.3 \times 10^{12} L_\odot$ and $1.2 \times 10^{12} L_\odot$, respectively. The discrepancy in the L_{IR} and $L_{8-155\,\mu m}$ values is expected, however, the fact that the two luminosities are so similar is evident in Figure 6; only a moderate contribution to the infrared luminosity is from emission redward of 155 μm.

5. DISCUSSION

With an estimated molecular gas mass of $5.7 \times 10^{10} \, M_\odot$, the PG 1700+518 system is one of the most molecular gas-rich QSO hosts thus far detected in CO(1 → 0) in the local universe. Its molecular gas mass is a factor of 2 greater than that of Mrk 1014 (= $2.5 \times 10^{10} \, M_\odot$; Evans et al. 2006), and is comparable to that of the host of the radio-loud quasar 3C 48 (= $5.8 \times 10^{10} \, M_\odot$; Scoville et al. 1993; Wink et al. 1997). It is also one of the most luminous (and hence massive) PG QSO systems in the local universe, having a host+companion H-band magnitude of $M_H \sim -26.13$ mag (Guyon et al. 2006) and a host-galaxy stellar bulge mass of $\sim 4 \times 10^{11} \, M_\odot$; the later quantity is derived by making use of the PG 1700+518 black hole mass measured via the reverberation technique ($M_\bullet = 7.81 \times 10^8 \, M_\odot$; Peterson et al. 2004) and the black hole-to-stellar bulge mass relation for nearby massive galaxies ($M_\bullet / M_* \sim 0.002$; Marconi & Hunt 2003; see also Magorrian et al. 1998). By comparison, Mrk 1014 (= PG 0157+001), PG 0804+761, and PG 1613+658, the three other high-luminosity (i.e., $M_B < -23.5$ mag) PG QSOs with published CO detections, have host magnitudes of $M_H \sim -26.01$ mag, -23.92 mag and -25.87 mag, respectively. Thus, these new observations provide another example of a $M_B < -23.5$ mag PG QSO with a massive, morphologically disturbed, molecular gas-rich host galaxy, and provide another counter-example to the claim that $M_B < -23.5$ mag QSOs and quasars reside (only) in giant elliptical galaxies (e.g., Dunlop et al. 2003). The local population of giant elliptical galaxies are observed, of course, to be deficient in molecular gas (Lees et al. 1991).

Aside from its relatively extreme CO and infrared luminosities, the general infrared and CO properties of the PG 1700+518 system are indistinguishable from the local CO-detected PG QSO population—the CO line width of $\Delta v_{\mathrm{FWHM}} \sim 260$ km s^{-1} and the measured infrared-to-CO luminosity ratio, $L_{\mathrm{IR}}/L'_{\mathrm{CO}}$,[16] of 340 $L_\odot$ (K km s^{-1} pc^2)$^{-1}$ are consistent with the average line width (= 280 ± 150 km s^{-1}) and $L_{\mathrm{IR}}/L'_{\mathrm{CO}}$ (= $350 \pm 175 \, L_\odot$ [K km s^{-1} pc^2]$^{-1}$) measured for other $z < 0.3$ PG QSO hosts detected in CO to date (e.g., Sanders et al. 1988a; Barvainis et al. 1989; Evans et al. 2001, 2006; Scoville et al. 2003).

A direct comparison between the CO properties of the PG 1700+518 system and the high-z QSO hosts detected thus far in CO is difficult due to unknown or possibly erroneous gravitational lensing amplification corrections of the high-z sample, and due to the fact that most high-z QSO hosts are observed in higher transitions of CO. However, by making use of the amplification factors compiled by Solomon & Vanden Bout (2005) and making reasonable assumptions about the ratio of the CO(2→1) and CO(3→2) luminosities relative to CO(1→0),[17] it is concluded that the molecular gas mass of PG 1700+518 system is on the low end of the range (= $1 - 30 \times 10^{10} \, M_\odot$, with a median value of $12 \times 10^{10} \, M_\odot$) of gas masses estimated for high-z QSO hosts. In terms of line widths, the PG 1700+518 system has a width comparable to the median line width (= 280 km s^{-1}) of the high-z QSO host sample. The dispersion of velocity widths for the high-z sample is

180 km s^{-1}, i.e., similar to that measured for the local QSO host sample.

5.1. The Host and Companion Galaxies

Unlike the majority of the other local QSO host galaxies detected in CO to date, PG 1700+518 clearly resides in a widely separated (7 kpc) double nucleus, apparently interacting, system. The WFPC2 and NICMOS images show the clearest view to date of both the host galaxy and the companion. The disturbed morphology of the host galaxy of the pair (e.g. Figure 3) is consistent with that observed many for infrared bright QSOs (e.g., Surace et al. 2001; Guyon et al. 2006), which are sometimes observed to have faint tidal tails.

In the case of the companion, the morphology and colors are consistent with those of collisional ring galaxies (e.g., see Table 1 of Hines et al. 1999 for a summary of local ring galaxies). In addition, the redness of the nucleus and relative blueness of the ring provide a natural explanation for the E + A spectral classification of the companion by Stockton et al. (1998; see also Canalizo & Stockton 1997). Although the evidence is consistent with the companion being a collisional ring galaxy, the possibility that the "ring" is actually a tidal tail associated with the companion cannot be ruled out completely with the present data set.

While Keck spectroscopy of the companion shows evidence of recent star formation (Canalizo & Stockton 1997), the redshift of the CO(1→0) emission line is consistent with optical redshifts measured for the QSO, and thus the CO appears to be associated with the QSO host galaxy and not with the companion. The data do not rule out the possibility that the companion is relatively molecular gas-rich—if the assumption is made that the CO emission from the companion galaxy has the same line width as the QSO host, the companion has a 3σ molecular gas mass upper limit of $3 \times 10^{10} \, M_\odot$, i.e., the companion galaxy could still be extremely gas-rich.

Further progress in ascertaining the molecular gas distribution of the QSO system could be made via follow-up CO and 1mm continuum observations with the IRAM Plateau de Bure interferometer. Such observations could be used to address three primary issues. First, the observations would allow the best possibility of obtaining high signal-to-noise CO observations of the companion galaxy at a resolution sufficient to spatially separate the CO emission associated with both galaxies. Second, the observations may aid in establishing whether the companion nucleus is red due to dust extinction or due to the presence of a well evolved stellar population. Third, the 1 mm continuum observations would provide some hint of whether the companion galaxy is a significant contributor to the thermal dust emission (and thus a significant source of infrared-submillimeter luminosity) of the PG 1700+518 system—the existing *IRAS*, *ISO*, and *Spitzer Space Telescope* imaging data at the MIR and FIR are too low resolution to spatially separate the host and companion.

5.2. Star Formation Rates and AGN Fueling

Given the richness of the ISM of the PG 1700+518 host, the obvious question to ask is—what is the star formation rate? This is a nontrivial and highly speculative exercise, primarily due to the difficulty of ascertaining what fraction of the infrared (or radio) emission is generated by the active galactic nucleus (AGN). A conservative upper limit on the star formation rate can be derived by assuming that the total light from the starburst

---

[16] The ratio $L_{\mathrm{IR}}/L'_{\mathrm{CO}}$ is the star formation "efficiency" if L_{IR} is produced solely by dust heated by the starburst population and L'_{CO} is tracing the fuel from which new stars are being created. However, see Section 5.2.

[17] We have adopted $L'_{\mathrm{CO}(2\to1)}/L'_{\mathrm{CO}(1\to0)} = 0.8$ (i.e., the ratio for the $z = 4.1$ QSO host of PSS J2322+1944; see Solomon & Vanden Bout 2005) and $L'_{\mathrm{CO}(3\to2)}/L'_{\mathrm{CO}(1\to0)} = 0.6$ (see Yao et al. 2003).

population, L_{SB}, is absorbed by dust and reradiated as the FIR emission of the PG 1700+518 system. Thus, Equation (4) of Kennicutt (1998) is used to calculate a star formation rate of

$$\dot{M}_* = 1.76 \times 10^{-10} \left(\frac{L_{FIR}}{L_\odot} \right) M_\odot \, \text{yr}^{-1} \approx 210 \, M_\odot \, \text{yr}^{-1}. \quad (4)$$

where $L_{FIR} = 1.2 \times 10^{12} \, L_\odot$, i.e., the 40–120 μm luminosity measured in Section 4 by integrating under the SED curve in Figure 6 (see Section 4). Note that for the PG 1700+518 system, L_{FIR} is 1/5 of the bolometric luminosity.

Another star formation rate tracer used over the past several years is the luminosity of MIR polycyclic aromatic hydrocarbon (PAH) emission, L_{PAH}. Shi et al. (2007) obtained *Spitzer Space Telescope* IRS observations of PG QSO hosts, radio galaxies, and 2MASS quasar hosts and calculate their L_{PAH}. By making the assumption that PAH emission in both starburst and AGN host galaxies trace star formation, Shi et al. use the starburst galaxy-derived L_{PAH}/L_{IR} ($\sim L_{PAH}/L_{SB}$) to estimate L_{SB} for the AGN hosts. For the PG 1700+518 host, they derive an upper limit of $L_{SB} < 6.5(\pm 2.6) \times 10^{11} \, L_\odot$, where the error represents the scatter in the L_{PAH}/L_{IR} relation for starburst galaxies. While their results raise the very real possibility that a negligible fraction of the L_{IR} is due to star formation, their results are also consistent with the assertion that the L_{FIR} is completely due to star formation.

In terms of MIR star formation and AGN diagnostics, it is also worth noting that the high ionization 14.3 μm [Ne v] emission line, observed in AGNs, is not detected in PG 1700+518 (Schweitzer et al. 2006; Netzer et al. 2007). The ratio of [Ne v] to the low-ionization [Ne ii] 12.8 μm emission line, [Ne v]/[Ne ii], is $\leqslant 0.2$, which is weak relative to the median value of [Ne v]/[Ne ii] = 1.4 measured for the 19 [Ne v]-detected QSO hosts in the Schweitzer et al. sample (the values range from [Ne v]/[Ne ii] = 0.29 to 5.51). Such a low value may be indicative of a host with an energetically weak AGN similar to NGC 6240 (Armus et al. 2006) and NGC 2623 (Evans et al. 2008) and thus support the idea that a large fraction of the L_{IR} is due to star formation. However, if the majority of the [Ne v]-emitting region of PG 1700+518 is blocked by a Compton thick absorber, as appears to be the case for the [Ne v] depleted Seyfert 1 galaxy Mrk 231 (Braito et al. 2004; Armus et al. 2007), the [Ne v]/[Ne ii] ratio provides little insight into AGN energetics.

Finally, another traditional way of estimating the star formation rates of galaxies is via the radio luminosity. The underlying assumption is that synchrotron emission from supernovae (SNe) is the cause of the emission measured at 1.5 GHz. This method does not work for the host of PG 1700+518; it lies at the upper end of the distribution of the infrared–radio correlation of starburst galaxies, and is thus moderately radio-loud. The 1.5 GHz flux density of PG 1700+518 is 21.6 ± 0.8 mJy (Condon et al. 1998), which translates into a luminosity of $P_{1.5GHz} \sim 4.8 \times 10^{24} \, \text{W Hz}^{-1}$, and thus $P_{1.5GHz}/L_{IR} \sim 1.0 \times 10^{12} \, \text{W Hz}^{-1} \, L_\odot^{-1}$. By comparison, the median $P_{1.5GHz}/L_{IR}$ of starburst galaxies is ~ 2–$3 \times 10^{11} \, \text{W Hz}^{-1} L_\odot^{-1}$ (e.g., see Figure 5 of Evans et al. 2005). Thus, a significant amount of its radio emission must be generated by processes associated with the AGN, and not star formation. Indeed, if one were to naively estimate a star formation rate with the radio luminosity using the prescription in Bell (2003), the resultant rate would be

$$\dot{M}_* = 5.52 \times 10^{-22} \left(\frac{L_{1.4GHz}}{\text{W Hz}^{-1}} \right) M_\odot \, \text{yr}^{-1} \approx 2650 \, M_\odot \, \text{yr}^{-1}, \quad (5)$$

i.e., a factor of 13 higher than $\dot{M}_*$ calculated via Equation (4). It is worth noting that the 5 GHz core-to-total radio emission of PG 1700+518 is 0.28 (Kellermann et al. 1989; see also Kellermann et al. 1994)—the value one would expect if the ratio of core-to-extended radio emission is equal to the ratio of AGN-to-SN radio emission is ~ 0.92. In other words, if the FIR emission traces the majority of the UV and optical emission from the starburst population, it is not simply a matter of using only the $L_{1.4GHz}$ of the extended emission to explain the $\dot{M}_*$ discrepancy between Equations (4) and (5)—the extended radio emission is heavily contaminated by the AGN.

If L_{FIR} is adopted as the total luminosity of the starburst population, then the QSO generates a luminosity of $\sim 3.6 \times 10^{12} \, L_\odot$ in the thermal infrared alone. This luminosity is equivalent to that estimated for the black hole of PG 1700+518 if it radiates at $\sim 14\%$ (i.e., $\eta \sim 0.14$) its Eddington Luminosity of

$$L_{edd} = \frac{4\pi G m_p c}{\sigma_T} M_\bullet = 3.2 \times 10^4 \left(\frac{M_\bullet}{M_\odot} \right) L_\odot \approx 2.5 \times 10^{13} \, L_\odot, \quad (6)$$

where G is the Gravitational constant, σ_T is the Thompson scattering cross section, c is the speed of light, m_p is the proton mass, and $M_\bullet$ is the black hole mass of $\sim 7.81 \times 10^8 \, M_\odot$ for PG 1700+518 estimated by Peterson et al. (2004) via reverberation mapping. Note, however, that the infrared luminosity of the AGN is a lower limit to the total luminosity attributable to the QSO. If the assumption is made that only the L_{FIR} contribution emanates from dust heated by stars in the host and that the rest of the L_{bol} is essentially associated with QSO emission/heating, i.e., $L_{bol} - L_{FIR} \sim 5.0 \times 10^{12} \, L_\odot$, then $\eta \sim 0.20$.

In terms of fueling rates, the QSO must consume

$$\dot{M}_\bullet = \frac{L_{AGN}}{\eta c^2} = 0.068 \left(\frac{L_{AGN}}{10^{12} L_\odot} \right) \frac{1}{\eta} M_\odot \, \text{yr}^{-1} \approx 1.7 \, M_\odot \, \text{yr}^{-1} \quad (7)$$

to maintain its present luminosity—i.e., the AGN consumes a negligible amount of gas relative to the amount consumed through star formation ($\sim 210 \, M_\odot \, \text{yr}^{-1}$). At the present rate of gas consumption, the starburst and AGN activity will consume the available fuel in $\sim 3 \times 10^8$ yr. If the value of α ($= M(H_2)/L'_{CO}$) is as low as 1 $M_\odot$ (K km s^{-1} pc^2)$^{-1}$, as has been proposed for many ultraluminous infrared (i.e., $L_{IR} \geqslant 10^{12} \, L_\odot$) galaxies in the local universe (Downes & Solomon 1998), then the gas consumption rate may be as short as $\sim 7 \times 10^7$ yr. Whether these fueling rate estimates are likely to increase or not is dependent on the effects of starburst and AGN feedback, as well as whether the companion galaxy is sufficiently bound to the QSO host to eventually fall inward. Such an event would result in the enhancement of gas compression, resulting in a dramatic increase in the star formation rate and a shorter gas depletion time.

Interestingly, PG 1700+518 is a member of the rare subclass of broad absorption line QSOs (BALQSOs) that exhibit absorption from low-ionization species (e.g., Al iii, Mg ii, Na i) in addition to absorption from high-ionization species (e.g., N v, Si iv, C iv; Turnshek et al. 1985; Pettini & Boksenberg 1985; Wampler 1985). It has been suggested that the low-ionization BALQSOs are either viewed at inclinations just skimming the edge of an optically thick torus (e.g., Murray et al. 1995; but see Punsly 2006), or have a higher covering fraction of gas and dust near the nucleus than non- and high-ionization BALQSOs, perhaps as a result of a recent event that has either perturbed an

existing molecular torus or has dumped new material onto the nucleus (e.g., Boroson & Meyers 1992). Given the large inferred molecular gas mass in PG 1700+518, evidence for a high-impact parameter collision between the QSO and its companion (see discussion in Hines et al. 1999), and the presence of absorbing gas and dust in the line-of-sight, perhaps we are witnessing the fueling event in progress with an accompanying expulsion of material along our line of sight in the form of BAL gas. The object may be emerging from a gas and dust enshrouded "cocoon phase" as envisioned by the scenario of Sanders et al. (1988b).

6. SUMMARY

New millimeter-wave CO(1→0) and *HST* optical and NIR observations of the PG 1700+518 system are presented. These observations provide the first detection of CO(1→0) in the system, and show the clearest view to date of the companion galaxy and the QSO host. The following conclusions are reached.

1. The QSO host system has an $L'_{CO} = 1.4 \times 10^{10}$ K km s^{-1} pc^2 and a derived molecular gas mass of $M_{H_2} \sim 5.7 \times 10^{10} \, M_\odot$ (adopting an $\alpha = 4 \, M_\odot$ [K kms^{-1}pc^2]$^{-1}$), making it one of the most molecular gas-rich PG QSO host systems observed in CO(1→0) to date.

2. Both the Δv_{FWHM} (= 260 km s^{-1}) and the L_{IR}/L'_{CO} (= 340 $L_\odot$ [K km s^{-1} pc^2]$^{-1}$) of the PG 1700+518 host system are comparable to the average values measured for other PG QSO hosts detected in CO(1→0) to date.

3. The host galaxy of PG 1700+518 has a bulge and an extended (11 kpc) tidal tail. Its companion has properties consistent with a collisional ring galaxy, however, the possibility that the "ring" is actually a tidal arm associated with the companion cannot be ruled out completely. The companion has a very red nucleus and a relatively bluer ring. The colors of the companion explain its E+A spectroscopic classification, and provide evidence that the young stellar population, with a spectroscopically derived age of 85 Myr, resides in the ring component.

4. It is concluded, based on the optical redshifts of the companion and the QSO emission-line region, that the observed CO emission is associated with the QSO host. However, based on the present data, a molecular gas mass of $\sim 10^{10} \, M_\odot$ for the companion galaxy cannot be ruled out.

5. A star formation rate for the QSO host of $\sim 210 \, M_\odot$ yr^{-1} is estimated based on the assumption that L_{FIR}, which is 1/5 of the bolometric luminosity, is the luminosity of the starburst population. Given this rate, the star formation and AGN activity in the host galaxy could be fueled from the available gas for another $\sim 10^8$ yr. These numbers are highly uncertain due to the unknown relative contributions of star formation and AGN activity to the infrared luminosity, the effects of feedback, or enhancements/suppression of star formation by the ongoing interaction.

REFERENCES

Appleton, P. N., & Marston, A. P. 1997, AJ, 113, 201
Armus, L., et al. 2006, ApJ, 640, 204
Armus, L., et al. 2007, ApJ, 656, 148
Bahcall, J. N., Kirhakos, S., & Schneider, D. P. 1995, ApJ, 450, 486
Barker, E., et al. 2007, "NICMOS Instrument Handbook," Version 10.0 (Baltimore, MD: STScI)
Barvainis, R., Alloin, D., & Antonucci, R. 1989, ApJ, 337, 69
Bell, E. F. 2003, ApJ, 586, 794
Boroson, T. A., & Meyers, K. A. 1992, ApJ, 397, 442
Braito, V., et al. 2004, A&A, 420, 79
Canalizo, G., & Stockton, A. 1997, ApJ, 480, L5
Condon, J. J., Cotton, W. D., Greisen, E. W., Yin, Q. F., Perley, R. A., Taylor, G. B., & Broderick, J. J. 1998, AJ, 115, 1693
Downes, D., & Solomon, P. M. 1998, ApJ, 507, 615
Dunlop, J. S., McLure, R. J., Kukula, M. J., Baum, S. A., O'Dea, C. P., & Hughes, D. H. 2003, MNRAS, 340, 1095
Evans, A. S., Frayer, D. T., Surace, J. A., & Sanders, D. B. 2001, AJ, 121, 3286
Evans, A. S., Mazzarella, J. M., Surace, J. A., Frayer, D. T., Iwasawa, K., & Sanders, D. B. 2005, ApJS, 159, 197
Evans, A. S., Solomon, P. M., Downes, D., Tacconi, L. J., & Vavilkin, T. 2006, AJ, 132, 2398
Evans, A. S., et al. 2008, ApJ, 675, L69
Griersmith, D., Hyland, A. R., & Jones, T. J. 1982, AJ, 87, 1106
Guyon, O., Sanders, D. B., & Stockton, A. 2006, ApJS, 166, 89
Hawkins, M. R. S. 1978, MNRAS, 182, 361
Heyer, et al. 2004, WFPC2 Instrument Handbook, Version 9.0 (Baltimore, MD: STScI)
Hines, D. C., Low, F. J., Thompson, R. I., Weynman, R. J., & Storrie-Lombardi, L. J. 1999, ApJ, 512, 140
Holtzman, J. A., Burrows, C. J., Casertano, S., Hester, J. J., Trauger, J. T., Watson, A. M., & Worthey, G. 1995, PASP, 107, 1065
Hutchings, J. B., Crampton, D., & Campbell, B. 1984, ApJ, 280, 41
Hutchings, J. B., Neff, S. G., & Gower, A. C. 1992, PASP, 104, 62
Kellermann, K. I., Sramek, R. A., Schmidt, M., Green, R. F., & Shaffer, D. B. 1994, AJ, 108, 1163
Kellermann, K. I., Sramek, R., Schmidt, M., Shaffer, D. B., & Green, R. 1989, AJ, 98, 1195
Kennicutt, R. C., Jr. 1998, ARA&A, 36, 189
Krist, J., et al. 1998, PASP, 110, 1046
Kristian, J. 1973, ApJ, 179, L61
Lees, J. F., Knapp, G. R., Rupen, M. P., & Phillips, T. G. 1991, ApJ, 379, 177
Lipari, S., et al. 2009, MNRAS, 392, 1295
Magorrian, J., et al. 1998, AJ, 115, 2285
Marconi, A., & Hunt, L. K. 2003, ApJ, 589, L21
Márquez, I., Petitjean, P., Théodore, B., Bremer, M., Monnet, G., & Beuzit, J.-L. 2001, A&A, 371, 97
Marston, A. P., & Appleton, P. N. 1995, AJ, 109, 1002
McLeod, K. K., & McLeod, B. A. 2001, ApJ, 546, 782
Murray, N., et al. 1995, ApJ, 451, 498
Netzer, H., et al. 2007, ApJ, 666, 806
Neugebauer, G., Green, R. F., Matthews, K., Schmidt, M., Soifer, B. T., & Bennett, J. 1987, ApJS, 63, 61
Papadopoulos, P. P., Kovacs, A., Evans, A. S., & Barthel, P. 2008, A&A, 491, 483
Persson, S. E., Frogel, J. A., & Aaronson, M. 1979, ApJS, 39, 61
Peterson, B. M., et al. 2004, ApJ, 613, 682
Pettini, M., & Boksenberg, A. 1985, ApJ, 294, L73
Punsly, B. 2006, ApJ, 647, 886
Rhoads, J. E. 2000, PASP, 112, 703

Sanders, D. B., & Mirabel, I. F. 1996, ARA&A, 34, 749
Sanders, D. B., Scoville, N. Z., & Soifer, B. T. 1988a, ApJ, 335, L1
Sanders, D. B., Soifer, B. T., Elias, J. H., Madore, B. F., Matthews, K., Neugebauer, G., & Scoville, N. Z. 1988b, ApJ, 325, 74
Schmidt, M., & Green, R. F. 1983, ApJ, 269, 352
Schneider, G., Silverstone, M. D., & Hines, D. C. 2005, ApJ, 629, L117
Schneider, G., et al. 1999, AJ, 121, 525
Schweitzer, M., et al. 2006, ApJ, 649, 79
Scoville, N. Z., Frayer, D. T., Schinnerer, E., & Christopher, M. 2003, ApJ, 585, L105
Scoville, N. Z., Padin, S., Sanders, D. B., Soifer, B. T., & Yun, M. S. 1993, ApJ, 415, L75
Shi, Y., et al. 2007, ApJ, 669, 841
Silk, J., Smith, H. E., Spinrad, H., & Field, G. B. 1973, ApJ, 181, L25

Skrutskie, M. F., et al. 2006, AJ, 131, 1163
Solomon, P. M., & Vanden Bout, P. A. 2005, ARA&A, 43, 677
Stickel, M., Fried, J. W., McLeod, K. K., & Rieke, G. H. 1995, AJ, 109, 1979
Stirpe, G. M. 1990, A&AS, 85, 1049
Stockton, A., Canalizo, G., & Close, L. M. 1998, ApJ, 500, L121
Surace, J. A., Sanders, D. B., & Evans, A. S. 2001, AJ, 122, 2791
Turnshek, D. A., Foltz, C. B., Weymann, R. J., Lupie, O. L., McMahon, R. G., & Peterson, B. M. 1985, ApJ, 294, L1
van Dokkum, P. G. 2001, PASP, 113, 1420
Veilleux, S., et al. 2006, ApJ, 643, 707
Wampler, E. J. 1985, ApJ, 296, 416
Wink, J. E., Guilloteau, S., & Wilson, T. L. 1997, A&A, 322, 427
Yao, L., Seaquist, E. R., Kuno, N., & Dunne, L. 2003, ApJ, 588, 771